FULL PAPER

Bioinspired Graphene Actuators Prepared by Unilateral UV Irradiation of Graphene Oxide Papers

Dong-Dong Han, Yong-Lai Zhang, Yan Liu, Yu-Qing Liu, Hao-Bo Jiang, Bing Han, Xiu-Yan Fu, Hong Ding, Huai-Liang Xu, and Hong-Bo Sun**

Inspired by natural autonomous systems that demonstrate controllable shape, appearance, and actuation under external stimuli, a facile preparation of moisture responsive graphene-based smart actuators by unilateral UV irradiation of graphene oxide (GO) papers is reported. UV irradiation of GO is found to be an effective protocol to trigger the reduction of GO; however, due to the limited light transmittance and thermal relaxation, thick GO paper cannot be fully reduced. Consequently, by tuning the photoreduction gradient, anisotropic GO/reduced GO (RGO) bilayer structure can be easily prepared toward actuation application. To get better control over the responsive properties, GO/RGO bilayer paper with a certain curvature and RGO patterns are successfully prepared for actuator design. As representative examples, smart humidity-driven graphene actuators that mimic the cilia of respiratory tract and tendril climber plant are successfully developed for controllable objects transport.

1. Introduction

Smart actuators are devices that can convert external stimulations such as light,[1] temperature,[2] pH value,[3] moisture,[4] magnetic/electric fields,[5] and chemicals[6] to visualized movements by fast, reversible and controllable structure/morphology changes.[7] Owing to the intelligent driving manner, smart actuators have received enormous research interests and already revealed great potential in emerging applications including adaptive optics,[8] intelligent robots,[9] unmanned vehicles,[10] lab-on-a-chip (LoC) systems,[11] and microelectromechanical systems.[12] Nowadays, smart actuators also hold great promise for developing the next-generation smart products, for instance, eco-friendly wearable computers, electronic skins, artificial muscles, and smart microrobots.[13] Without any energy supply systems or coupled instruments, smart actuators would act as an intelligent component to realize desired performance such as haptic stimulus,[14] targets capture/release,[15] and biomimetic actuations[16] in a controllable manner. Triggered by these unique advantages, great efforts have been devoted to rational design and fabrication of smart actuators based on various material systems. As typical examples, Gracias et al., successfully proposed a series of bilayer self-folding devices such as gripping devices and containers that could be manipulated by laser,[17] temperature,[18] chemicals,[19] and even enzymes.[20] However, despite the big success, concerns with respect to mechanical stabilities between different material layers constitute a main barrier for their practical applications, especially with excessive use. In this regard, current trend that integrates new mechanical designs into actuation systems is opening new horizons for new-style advanced actuators.

In the pursuit of novel smart actuators, light-weight and inexpensive carbon materials have been widely chosen as preferred candidates due to their fascinating characteristics such as mechanical robustness, chemical/physical stabilities, and high dimension variation properties.[21] Especially, as a new member of the carbon family, graphene and its related materials (e.g., graphene oxide, GO) are very promising for smart actuators, since they exhibit enticing physical/chemical properties (e.g., extraordinary mechanical strength, conductivity, flexibility, large surface area, thermal conductivity, and excellent biocompatibility)[22] and broad perspective.[23] In view of these fascinating superiorities, graphene-based smart actuators based on a solo carbon material have been successfully proposed and are currently being developed for both fundamental and applied studies. For instance, Qu et al., successfully prepared the fiber-type smart actuators and robots by laser reduction of GO fibers.[24] Recently, we reported a simple photoreduction method to construct GO/reduced GO (RGO) bilayer actuators using focused sunlight irradiation.[25] However, despite

D.-D. Han, Prof. Y.-L. Zhang, Y.-Q. Liu, H.-B. Jiang, B. Han, X.-Y. Fu, Prof. H.-L. Xu, Prof. H.-B. Sun
State Key Laboratory on Integrated Optoelectronics
College of Electronic Science and Engineering
Jilin University
2699 Qianjin Street, Changchun 130012, China
E-mail: hbsun@jlu.edu.cn;
yonglaizhang@jlu.edu.cn
Prof. Y. Liu
Key Laboratory of Bionic Engineering (Ministry of Education)
Jilin University
Changchun 130022, China
Prof. H. Ding
State Key Laboratory of Inorganic Synthesis and Preparative Chemistry
College of Chemistry
Jilin University
Changchun 130012, China
Prof. H.-B. Sun
College of physics
Jilin University
Changchun 130012, China

DOI: 10.1002/adfm.201501511

the anisotropic treatments impart stimuli-responsive properties to the resultant graphene actuators, the pinpoint photoreduction of GO with respect to both direct laser writing[26] and focused sunlight irradiation significantly lower the fabrication efficiency; it is almost impossible to produce such graphene actuators on a large scale. Additionally, the scanning processing manner also makes the GO/RGO bilayer not uniform, leading to unstable response under external stimulus. More importantly, the response of such actuators is usually limited to simple bending and straightening; more complex performance is almost impossible. Currently, the researches on graphene actuators are still open for innovative technologies that permit facile, high-efficiency, and large scale production of stimuli responsive graphene structures that can perform complex actions.

Herein, we reported a facile preparation of humidity-driven graphene actuators by unilateral UV irradiation of GO papers. Surface properties of the GO paper could be drastically changed after UV irradiation for tens of minutes due to the photoreduction effects, in which most of the oxygen-containing groups (OCGs) on GO sheets have been removed. Taking advantage of the photoreduction gradient that is dominated by light transmittance and thermal relaxation, thick GO paper could not be fully reduced. Consequently, a self-controlled photoreduction process could be easily achieved, yielding anisotropic GO/RGO bilayer structures that could be driven by moisture. To get better control over their responsive properties, GO/RGO bilayer paper with a certain curvature and a flat one with RGO patterns have been successfully prepared. As typical examples, smart humidity-driven graphene actuators that mimicked the cilia of respiratory tract and tendril climber plant have been developed for controllable objects transport.

2. Results and Discussion

2.1. Design Principle

As a chemical-free and highly efficient reduction strategy, photoreduction of GO has been widely used for the production of graphene, since it permits exquisite control over the content and the distributions of OCGs on GO sheets. Pioneer works with respect to radiation-induced GO reduction show that various radiation sources (e.g., sunlight, UV light, and laser) are workable for the removal of OCGs on GO sheets[27] or for inducing obvious chemical transformation on graphene-related materials.[28] Kumar et al. even observed the photothermal effects by measuring the temperature change during the radiation-induced chemical transformation.[28a] Based on the wavelength of incident light, the mechanism for photoreduction of GO could be briefly classified into photochemical reduction and photothermal treatment.[29] According to threshold argument reported by Smirnov et al., photon energies larger than 3.2 eV (λ < 390 nm) could trigger GO reduction through a photochemical process.[30] Consequently, in this work, we use UV light with a central wavelength of 365 nm as light source to reduce GO. The basic design principle of our GO/RGO bilayer structure is illustrated in **Scheme 1**. The mechanically flexible GO paper was prepared by vacuum filtration of GO aqueous solution; a free-standing GO paper was obtained after drying in air at room temperature. Despite the fact that UV light can trigger the reduction of GO sheets, photoreduction reaction in the interlayer of GO paper would be effectively suppressed due to the limited light transmission and thermal relaxation, as a result, OCGs on the surface layer of GO could be removed; whereas the bottom layer survived as pristine GO. To prove this hypothesis, we measured the transmittance spectra of GO paper of different thickness (Figure S1, Supporting Information). Thick GO films prevent light transmittance effectively. UV light with a central wavelength of 365 nm could be fully absorbed when the film thickness reaches 1.5 μm. In this case, a self-controlled photoreduction of thick GO film could be achieved without the use of any chemical additives or shadow masks. Taking advantage of this self-controlled photoreduction strategy, we designed and fabricated three typical bilayer structures, including a flat GO/RGO bilayer (GO/RGO-1), a curving GO/RGO bilayer (GO/RGO-2), and a patterned GO/RGO structures, for rational design of smart actuators. In our previous study, we have investigated the interaction between water molecules and single layer GO/graphene sheets.[31] Generally, GO sheets and water molecules could form hydrogen bond due to presence of OCGs; whereas the interaction between water and graphene sheets is much weaker Van der Waals force. According to this result, it is reasonable to deduce that GO would show much higher adsorption capacity of water molecules than that of RGO. Since the adsorption of water in the GO layer could induce obvious expansion, the asymmetric GO/RGO structure would lead to unsymmetrical deformation in humidity due to the different water adsorption capabilities. This hypothesis is in good agreement with our experimental phenomenon, as shown in the inset of Scheme 1. In our experiments, the initial curvature of GO paper could be flexibly determined using curving substrates with diverse curvatures, so the bending degree of the resultant GO/RGO bilayer structure could be tuned freely in a wide range (Scheme 1b). Additionally, with the help of masks, the radiation-induced photoreduction could be used for making RGO patterns on the GO paper.[32] Through rational design, the patterned GO/RGO bilayer structure can perform more complex actions, for instance, the wave-shaped deformation. (Scheme 1c).

2.2. Characterization of GO/RGO Bilayer Paper

First, we examined the section morphology of the GO paper before and after UV irradiation, as shown in **Figure 1**a,b. Cross-section scanning electron microscope (SEM) image of the GO paper shows stacked GO sheets with clear layered structure. The thickness of the GO paper was ≈6.5 μm. The top view SEM image reveals that the GO surface is very flat, only some wrinkles could be observed (inset of Figure 1a). By contrast, after UV treatments for 90 min, the surface became rough; and randomly distributed folds formed all over the RGO side (inset of Figure 1b). Section view of the GO/RGO paper showed that the stacked GO sheets were efficiently exfoliated from the upside layer which was exposed to UV light; and the bottom layer were still well stacked. In this case, a GO/RGO bilayer structure formed by simple UV irradiation. The obvious expansion

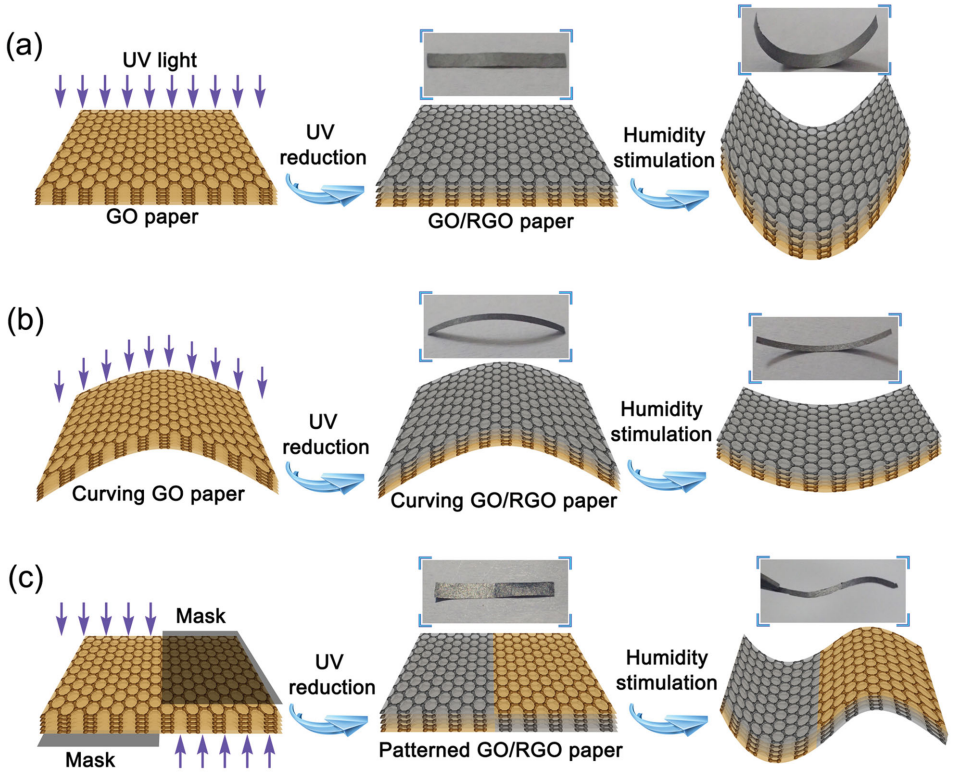

Scheme 1. Schematic illustration of the design principle of GO/RGO bilayer actuators, including a) flat GO/RGO paper, b) curving GO/RGO paper, c) patterned GO/RGO paper, and their predictable responsive properties to environmental humidity. The insets are digital photographs of GO/RGO bilayer ribbons in dry and moisture conditions.

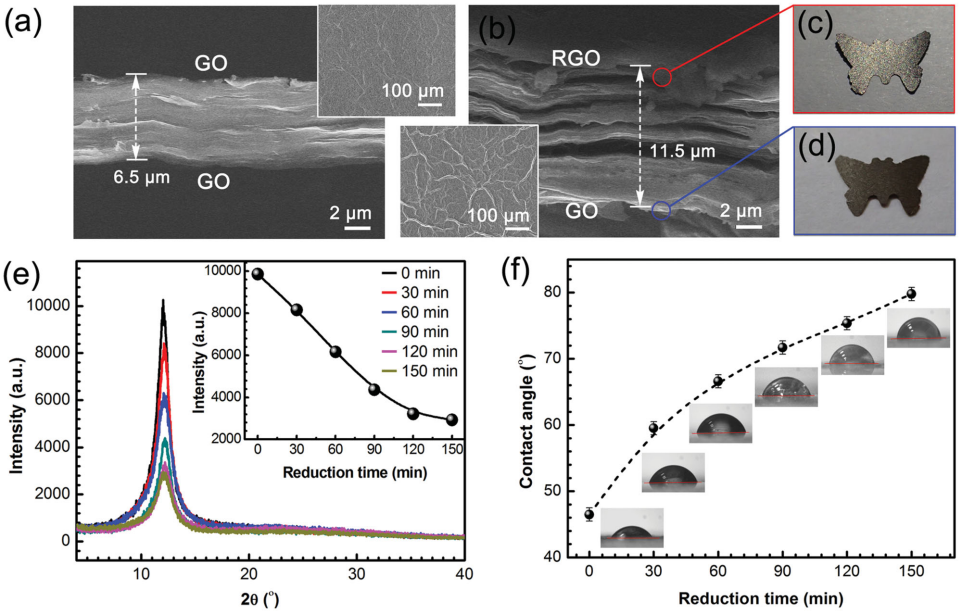

Figure 1. a) Cross section SEM image of pristine GO, the inset is SEM image of its surface; b) cross section SEM image of GO/RGO-1 bilayer structure, the inset is its RGO surface; c,d) photographs of the resultant GO/RGO bilayer viewed from the front side c) and the reverse side d), respectively; e) XRD patterns the RGO side of the bilayer paper prepared by UV irradiation for different time. The inset shows the intensity evolution of the diffraction peak at $2\theta = 11.9°$. f) The wettability change of the RGO surface versus different UV irradiation time.

in the RGO region could be attributed to the photoreduction-induced emission of carbon species (e.g., CO_2, CO)[33]; the film thickness grew to ≈11.5 µm, which corresponds to ≈75% expansion. Since the thickness of the GO/RGO paper increased with irradiation, we investigate the thickness ratio between the RGO layer and the whole GO/RGO paper (d_{RGO}/d_{Total}) to evaluate the reduction depth. As shown in Figure S2 (Supporting Information), with the increase of irradiation time, the RGO portion (d_{RGO}/d_{Total}) increased from 0 for pristine GO paper to 0.85 with respect to that after 150 min irradiation, indicating the gradually increased reduction depth. The UV reduction could be easily identified by the obvious color changes (Figure 1c,d). After UV reduction, the dark brown GO paper turned to black with a metallic luster; whereas the back side still remained the dark brown color, which suggests the reduction gradient along the lateral section.

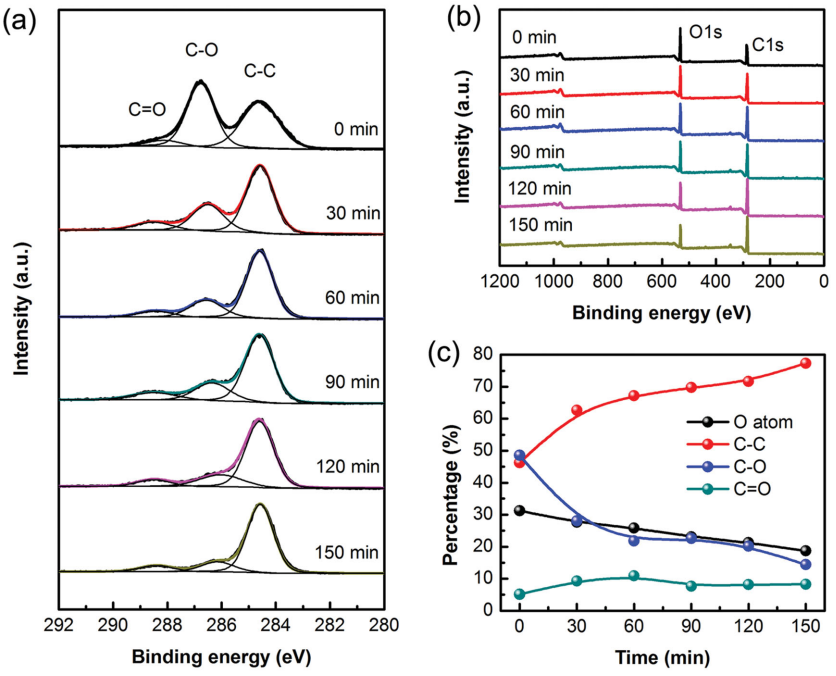

Figure 2. a) C1s XPS spectra of the pristine GO paper and the GO/RGO bilayer paper prepared by UV irradiation for different time, from 0 to 150 min; b) survey spectra of the GO paper and the GO/RGO bilayer paper; and c) dependence of C—C, C—O, C═O, and O atom percentage of the GO/RGO bilayer paper on UV irradiation time.

To evaluate the structure change upon UV irradiation, we measured the X-ray diffraction (XRD) patterns of the GO paper irradiated by UV light for different time, from 0 min with respect to pristine GO to 150 min. As shown in Figure 1e, with the increase of irradiation time, the diffraction peak at $2\theta = 11.9°$, which corresponds to a *d*-spacing of 7.4 Å between the stacked GO sheets, became weaker and weaker. The peak intensity decreased as a linear function of reduction time (inset of Figure 1e), especially in the first 2 h, which indicates that the RGO layer became disorder after the removal of OCGs. These results reveal that GO paper could be reduced in a controlled manner by simply varying the UV irradiation time. Similar with the reduction degree, the surface wettability of the RGO surface could also be modulated by irradiation time. As shown in Figure 1f, the pristine GO paper has a low water contact angle (CA) of 46°, indicating its hydrophilic nature. After UV irradiation for different time, CAs of the RGO side increase monotonically and finally reached a value of 80°. It is well known that the surface wettability was governed by both surface roughness and the chemical composition.[34] Considering the surface roughness change is not obvious, the increase in hydrophobicity after UV treatments could be mainly attributed to the decrease in surface energy, which was caused by the removal of hydrophilic OCGs.

We also investigate the photoreduction effect on the GO paper during UV irradiation. In our experiments, the color of GO paper gradually changed from yellow brown to black with the increase of UV irradiation time, which indicates the reduction of GO. To get further insight into the dependence of photoreduction degree on UV irradiation time, we investigate the X-ray photoelectron spectroscopy (XPS) of the RGO layers treated by UV irradiation for different time. Typically, C1s spectra of RGO films could be deconvoluted into three peaks that correspond to C—C (nonoxygen ring), C—O (hydroxyl and epoxy carbon), and C═O (carbonyl) at 284.6, 286.5, and 288.5 eV, respectively (**Figure 2**a). With the increase of UV irradiation time, the C—O and C═O peaks decreased, while the C—C peak increased, indicating the removal of OCGs. The survey spectra show a more obvious comparison (Figure 2b), the significantly decreased O 1s peaks and the increased C 1s peaks reveal that the photoreduction degree could be precisely controlled by irradiation time. Notably, for pristine GO, OCGs are very rich; the content of oxygen atoms is as high as 31.2% and the content of carbon not bonded to oxygen is only 46.3%. After UV reduction, the oxygen content decreased gradually to 18.7%; and the content of carbon not bonded to oxygen grows to 77.3%, indicating the dynamic reduction process. (Figure 2c). As compared with GO whose C/O atom ratio is only 2.2, the RGO film prepared after UV irradiation for 150 min shows a C/O atom ratio of 4.4, indicating the effective reduction of GO. Notably, significant decrease of C—O could be observed in the first hour, which reveals that OCGs containing C—O is much easier to remove under UV irradiation. Besides, Fourier transform infrared (FT-IR) spectra also give similar results (Figure S3, Supporting Information), the intensity of characteristic vibration bands such as hydroxyl and epoxyl groups (e.g., $\nu_{phenolic}$ at 1230 cm^{-1} and ν_{C-O} at 1050 cm^{-1}) decreased more obviously with the increase of irradiation time. They almost disappeared after UV irradiation for 90 min.

In fact, both UV light intensity and irradiation time show obvious influence on the extent of reduction. To get further insight into dynamic process, we investigated the FT-IR spectra of the RGO samples reduced under different light intensity and for different time. As shown in Figure S3 (Supporting Information), the increase of light intensity from ≈10 mW cm^{-2}

(300 W) to ≈30 mW cm^{-2} (500 W) would lead to a more thorough reduction of GO. Similarly, extent of reduction could also be controlled by irradiation time. When we gradually increased the reduction time from 30 to 150 min, the intensity of characteristic vibration bands include a strong C═O peak (1740 cm^{-1}), an O—H deformation peak around 1420 cm^{-1}, a C—OH stretching peak around 1230 cm^{-1} and a C—O stretching peak around 1050 cm^{-1} decreased markedly, some of them almost disappeared after long time irradiation. These results show that both light intensity and irradiation time could be tuned to get better control over the extent of GO reduction.

Besides, Raman spectra were taken on both pristine GO and RGO film that has been treated by UV irradiation for 90 min (Figure S4, Supporting Information). Two pronounced peaks at ≈1338 and 1598 cm^{-1} are observed in the spectra, corresponding to a disorder-induced feature (D-band) and the E_{2g} mode of graphite (G-band).[26] GO exhibited the higher I_D/I_G intensity ratio of ≈1.37; whereas the corresponding ratio for the RGO is only ≈0.94. The significantly decreased D band peak indicates the removal of oxygen defects and the partial recovery of sp^2 carbon after UV reduction.

2.3. Moisture Responsive Properties

As discussed previously, GO/RGO bilayer structure formed after unilateral UV reduction. Interestingly, when the GO/RGO bilayer paper was exposed to moisture, it curves due to the water-adsorption-induced expansion of GO layer. As shown in **Figure 3**a, most of the OCGs in RGO layer have been removed after UV reduction, whereas in the GO layer, plenty of OCGs survived. Since the presence of OCGs accounts for the adsorption of water in moisture, the anisotropic water adsorption with respect to the two layers would induced quite different swelling effects. Along the lateral direction, the interlayer spacing of the GO sheets would become larger obviously.[25] On the contrary, the RGO layer has negligible changes due to

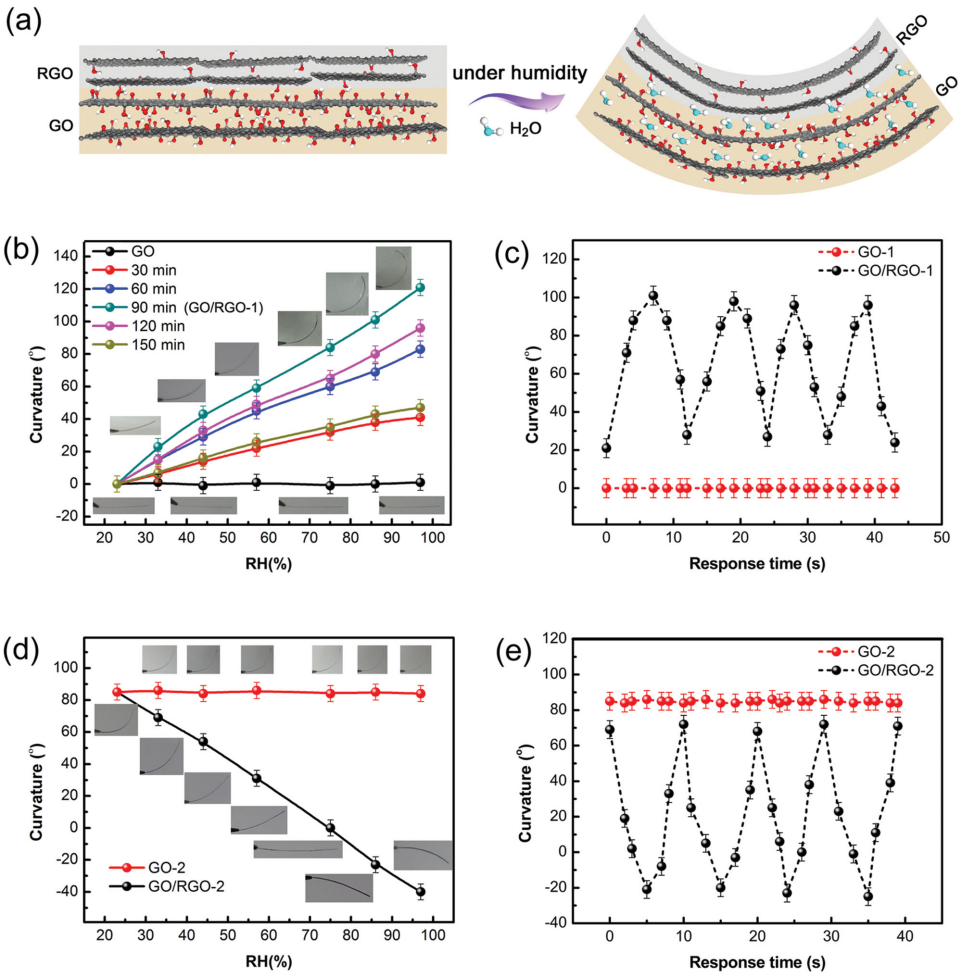

Figure 3. a) Schematic illustration of the bending behavior of the GO/RGO bilayer structure. Oxygen atoms in water have been demonstrated in different color for ease of identification. b) Bending angles curves for GO paper and different GO/RGO bilayer papers. The insets are photographs of GO and GO/RGO-1 ribbons under different humidity. c) Reversible response of GO/RGO-1 sample and its comparison with GO. RH was switched between 33% and 86%. d) Dependence of the curvature of curving GO and GO/RGO-2 samples on different RH. e) Reversible response of GO/RGO-2 sample and its comparison with curving GO. RH was switched between 33% and 86%.

very low water adsorption. It is known that pristine monolayer graphene prepared by mechanical exfoliation shows Young's modulus of ≈1.0 TPa and the ultimate breaking strength of ≈130 GPa;[35] whereas monolayer graphene oxide was found to have a lower effective Young's modulus (207.6–23.4 GPa) as compared with pristine graphene.[36] In the case of GO layer, according to Shenoy's results,[37] mechanical properties of GO paper are controlled by hydrogen bond networks that involve OCGs on individual GO platelets and water molecules within the interlayer cavities. The distinct expansion in the GO layer due to water adsorption will enlarge the interlayer spacing, and then GO sheets glide along the vertical direction to accommodate more water molecules. In this way, the GO/RGO ribbon curves under high humidity. Additionally, water content controls both the extent and collective strength of these interlayer hydrogen bond networks, contributing to the good mechanical performance.

In our experiments, by tuning the UV irradiation time, the reduction degree could be well controlled; this directly provides us an opportunity to further tune their bending performance. Typically, GO/RGO bilayer ribbons (12 mm × 1 mm) prepared by UV irradiating for different time (0–150 min) were exposed to moisture environment with different relative humidity (RH, 24%–97%); and the curving angles have been recorded. As shown in Figure 3b, with the increase of RH, all of the GO/RGO bilayer ribbons curve to higher degree through a quasi-linear dependence. However, for comparison, pristine GO ribbon did not show obviously change in moisture due to the isotropy in lateral section. When RH is as high as 97%, the highest curvature of ≈120° was observed in the case of GO/RGO ribbon prepared by UV irradiation for 90 min, which was denoted as GO/RGO-1. The insets show the photographs of the curving GO/RGO ribbons (90 min irradiation) under different RH. Here, it is important to point out that precise control of the proportion between GO and RGO is essential to achieve better actuating performance because the bending of GO/RGO bilayer originates from anisotropic water adsorption in the GO layer. In this regard, the bending behavior could be optimized by simply tuning the UV irradiation time. According to our results, UV reduction for 90 min (GO/RGO paper with a d_{RGO}/d_{Total} ratio of ≈0.6) is a suitable condition for the preparation of actuators with obvious response. This result gives us a hint that GO and RGO layer with similar thickness would be better for actuator design. However, the parameters are not invariable; it further depends on the thickness of pristine GO films and the dose of UV radiation.

Additionally, the bending performance is reversible; by altering the RH between 33% and 86%, bending and straightening performance could be switched freely from ≈25° to 100° (Figure 3c). Both the bending and straightening processes show fast response, the average response time for bending and straightening between 33% and 86% RH is measured to be 7 and 5 s, respectively. Moreover, the GO/RGO bilayer also shows excellent stability during frequent bending–unbending actuation, and the curvature almost keeps a consistent value, indicating the good reproducibility and precision of the actuation function. The response degree is so stable that no obvious deterioration could be observed after 100 cycles (Figure S5, Supporting Information). To quantificationally evaluate the bending/straightening force, the GO/RGO ribbon with the same size has been used for burden tests; the average bending and straightening forces were measured to be ≈0.63 and ≈0.35 mN, respectively. In fact, the bending force is dominated by the size and the thickness of the GO/RGO ribbon, a lager force could be obtained using wider GO/RGO ribbons.

To further extend the bending/straightening range, the curving degree of GO/RGO bilayer structure could be tuned in a much larger range using precurved GO papers. As a represent example, GO paper with an initial curvature of ≈85° was used for UV reduction; the resultant bilayer ribbon was denoted as GO/RGO-2. Similarly, with the increase of RH from 24% to 97%, the curvature of GO/RGO-2 ribbon changed from previous ≈85° to −39°, gradually. In this way, the GO/RGO-2 ribbon could be driven to bend toward the opposite direction (insets of Figure 3d). The curving degree also has a linear dependence on the environmental humidity (Figure 3d). For comparison, the curving GO ribbon was also exposed to moisture; however, the GO ribbon also keeps a constant curvature under different RH. Likewise, the bending and straightening processes of GO/RGO-2 also displayed a fast and reversible response. As shown in Figure 3e, bending and straightening could be freely switched by altering the RH between 33% and 86%.

Unlike the multilayer structures prepared by multimaterial deposition, GO/RGO bilayer paper could ensure a mechanically coherent GO/RGO interface since the bilayer structure are essentially based on the same material and the reduction degree is gradually changed along the lateral section. As a typical example, the distributions of OCGs along the lateral section were studied using XPS. We mechanically exfoliated the GO/RGO-1 paper into several layers; and in this way, the OCGs contents of the interlayers (different depth) could be easily measured. As shown in **Figure 4**a, with the increase of depth from the surface (RGO layer, 0 μm) to the bottom (GO layer), carbon atoms that bond to oxygen (C—O, C═O) increase obviously, indicating the anisotropic reduction degree along the lateral section. The XPS survey spectra of the surface layer and interlayers revealed an upward trend in oxygen and a downward trend in carbon signals (Figure 4b). The dependence of C—C, C—O and C═O contents on the reduction depth have been summarized in Figure 4c. The tendency is very clear, that is oxygen contents increased from surface to bottom. Typically, the contents of C—C and C—O gradually changed and became constant in the depth of ≈6.5 μm, which corresponds to the total thickness of the RGO layer. The above-mentioned XPS results confirm the photoreduction gradient and the anisotropic structure from the viewpoint of chemical compositions.

2.4. Bioinspired Actuators

The unique anisotropic structure enables rational design of smart graphene actuators based on this GO/RGO bilayer papers. As an interesting illustration, we fixed a GO/RGO-1 bilayer ribbon on a picture, which was designed as a "smart face," as shown in **Figure 5**a. Interestingly, when environmental humidity increased, it becomes a smile face; on the contrary, when the RH decreased, the face recovered. In a similar way,

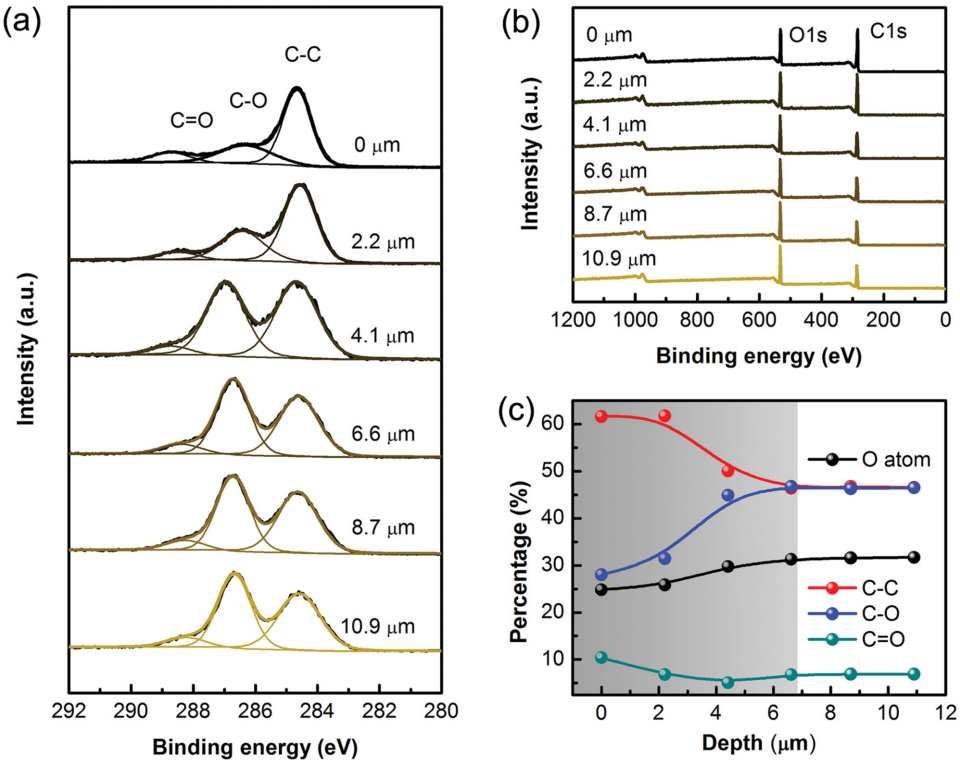

Figure 4. a) C1s spectra and b) Survey XPS spectra of GO/RGO-1 paper measured from surface to interlayers with different depth. c) C—C, C—O, C═O, and O atom percentage as a function of depth.

when a curving GO/RGO-2 ribbon was applied to the smart face, it can "smile" in low RH and become "unhappy" in high RH (Figure 5b).

Besides, inspired from the cilia of respiratory tract that can sweep tiny particles and hinder bacterial accumulation; we demonstrated smart humidity-driven graphene cilia using GO/RGO-1 and GO/RGO-2 ribbons. As introduced previously, the former ribbons (GO/RGO-1) bend up in moisture; whereas the later ribbons (GO/RGO-2) operate in the reverse mode, straightening in moisture. By assembling these two kinds of ribbons into two arrays on both sides of a gap (≈2 cm), a smart graphene-cilia actuator that mimics respiratory tract has been fabricated. As shown in Figure 5c, it could be driven by altering the environmental humidity; a paper cylindrical could be swept from the top of image to the bottom. In a typical process, the cilia array (GO/RGO-1) on the left side swept the object to lower right under high humidity; while when the humidity decreased, the cilia array (GO/RGO-2) on the right side swept the object lower left. In this manner, the smart actuator could be used for object transport. After three cycles, the target paper cylindrical shell moved ≈12 mm (Video 1, Supporting Information).

Inspired from tendril climber plants that can stretch out and twine round any suitable support using their helical tendril, we designed and prepared a smart graphene "tendril" by making RGO diagonal stripes on a GO ribbon (Figure S6, Supporting Information). The basic design principle is shown in **Figure 6**a, the RGO diagonal stripes were prepared by UV irradiation with the help of a mask. Interestingly, the GO/RGO ribbon curves under room humidity and curls to helical structure under high humidity (insets of Figure 6a). By attaching the graphene "tendril" to a plastic tube which is connected to moisture, a smart humidity driven graphene manipulator was proposed. It can twine round objects under high humidity and release them in dry air (Figure 6b and Video 2, Supporting Information). It is very important to point out that the development of smart graphene actuators based on our GO/RGO paper is not limited to such models. Through rational design of the curvature or the patterns of the GO/RGO papers, multifunctional humidity-driven graphene actuators could be readily fabricated.

3. Conclusion

In conclusion, a novel unilateral UV reduction of GO papers have been developed for facile and large-scale production of GO/RGO bilayer papers toward rational design and fabrication of graphene-based actuators. Due to the limited UV light transmittance and thermal relaxation, thick GO paper could not be fully reduced, and thus a self-controlled photoreduction gradient could be realized, yielding anisotropic GO/RGO bilayer structures. Very interestingly, the GO/RGO bilayer paper was very sensitive to moisture; it bends to the RGO direction due to the selective adsorption of water in the GO layer. To get better control over the responsive properties, GO/RGO bilayer paper with a certain curvature and various RGO patterns have been successfully prepared. Inspired from cilia of respiratory tract

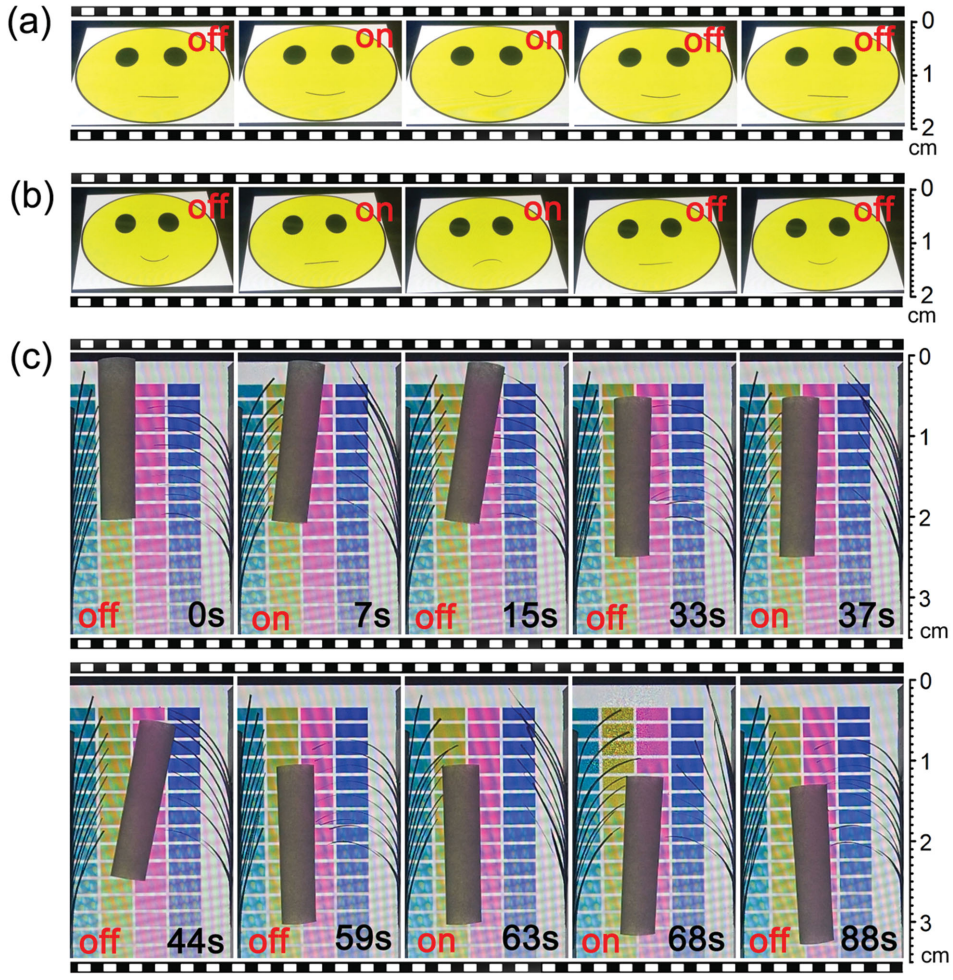

Figure 5. a,b) Moisture-responsive "smart face" using GO/RGO-1 a) and GO/RGO-2 b) ribbon as "mouth," respectively. b) Smart graphene "cilia" prepared by GO/RGO-1 (left) and GO/RGO-2 (right) ribbon arrays. The smart cilia could be used to sweep a paper cylindrical shell. "On" and "off" means turning on and turning off the humidity, respectively.

and the tendril climber plant, humidity-driven graphene actuators including a smart graphene "cilia" that can sweep objects and a graphene "tendril" that can capture/release target objects have been successfully developed, respectively. We deem that the unilateral UV photoreduction of GO paper in combination with UV lithography technology may enable rational design and flexible fabrication of various smart graphene actuators.

4. Experimental Section

Preparation of GO Paper: GO was synthesized by a modified Hummers method from natural graphite powder (Aldrich, <150 μm). GO paper was prepared by vacuum filtration of the GO aqueous solution through a membrane filter (0.22 μm in pore size), followed by air drying at room temperature. Curving GO paper was dried on curving substrates. Finally, the GO papers were peeled off for further use.

Preparation of GO/RGO Bilayer Papers: GO/RGO bilayer papers were prepared by unilateral UV irradiation of GO papers. XPA-Photochemical Reactor (Xujiang Electromech-anical Plant, Nanjing, China) with a 500 W medium pressure mercury lamp was used as UV light source, the light intensity on the sample surface is ≈30 mW cm^{-2} and the characteristic wavelength is 365 nm. The flat and curving GO papers were treated with UV irradiation for 30, 60, 90, 120, and 150 min at room temperature, respectively. Masks have been used for the patterning of GO/RGO papers.

Characterization: SEM images were obtained using a JEOL JSM-7500 field-emission scanning electron microscope (FE-SEM). The film thicknesses for GO papers were measured by atomic force microscopy (Digital Instruments Nano Scope III a) in the tapping mode. UV–vis transmittance spectra were measured by using a UV–vis spectrophotometer (UV-2550, SHIMADZU). Powder XRD patterns were collected on a Rigaku D/MAX 2550 diffractometer with Cu Kα radiation (λ = 1.5418 Å). The water CAs were measured using a Contact Angle Meter SL200B (Solon Tech. Shanghai). XPS was performed using an ESCALAB 250 spectrometer. Raman spectroscopy were recorded on a Jobin–Yvon T64000 Raman spectrometer equipped with a liquid-nitrogen-cooled argon ion laser at 514.5 nm (Spectra-Physics Stabilite 2017) as the excitation source; the laser power used was about 10 mW at the samples with an average spot size of 1 μm in diameter. The controlled humidity environments were achieved using saturated aqueous solutions of CH_3COOK, $MgCl_2$, K_2CO_3, NaBr, NaCl, KCl, and K_2SO_4 in a closed glass vessel, which yielded ≈23%, 33%, 44%, 57%, 75%, 86%, and 97% RH, respectively. All of the measurements were conducted in air at room temperature.

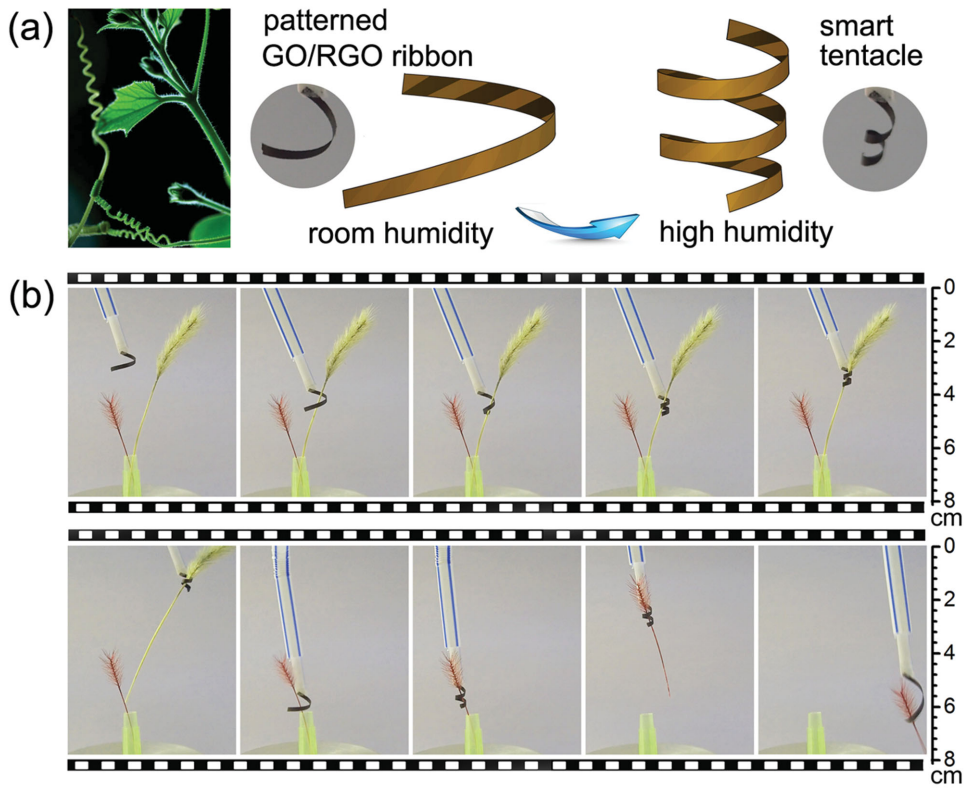

Figure 6. a) Schematic illustration of smart graphene "tendril" inspired from tendril climber plant (left image); the patterned GO/RGO ribbon with diagonal stripes was prepared by UV irradiation with the help of a mask; it curves under room humidity (≈30% RH, middle images) and curls to helical structure under high humidity (97% RH, right images). b) The smart graphene "tendril" was adhibited to a tube that is connected to moisture. In this way, it could be used for picking up and releasing objects.

Supporting Information

Supporting Information is available from the Wiley Online Library or from the author.

Acknowledgements

The authors would like to acknowledge the National Basic Research Program of China under Grant Nos. 2011CB013000 and 2014CB921302 and the National Natural Science Foundation of China (NSFC) under Grant Nos. 61376123, 61435005 and 51475200) for support.

Received: April 15, 2015
Revised: May 25, 2015
Published online: June 16, 2015

[1] a) S. Kawata, H. B. Sun, T. Tanaka, K. Takada, *Nature* **2001**, *412*, 697; b) M. Y. Ji, N. Jiang, J. Chang, J. Q. Sun, *Adv. Funct. Mater.* **2014**, *24*, 5412.
[2] K. Malachowski, M. Jamal, Q. R. Jin, B. Polat, C. J. Morris, D. H. Gracias, *Nano Lett.* **2014**, *14*, 4164.
[3] Y. L. Sun, W. F. Dong, R. Z. Yang, X. Meng, L. Zhang, Q. D. Chen, H. B. Sun, *Angew. Chem. Int. Ed.* **2012**, *51*, 1558.
[4] H. H. Cheng, Y. Hu, F. Zhao, Z. L. Dong, Y. H. Wang, N. Chen, Z. P. Zhang, L. T. Qu, *Adv. Mater.* **2014**, *26*, 2909.
[5] a) H. Xia, J. A. Wang, Y. Tian, Q. D. Chen, X. B. Du, Y. L. Zhang, Y. He, H. B. Sun, *Adv. Mater.* **2010**, *22*, 3204; b) G. Rydzek, T. G. Terentyeva, A. Pakdel, D. Golberg, J. P. Hill, K. Ariga, *ACS Nano* **2014**, *8*, 5240.
[6] M. Jamal, A. M. Zarafshar, D. H. Gracias, *Nat. Commun.* **2011**, *2*, 6.
[7] P. Brochu, Q. B. Pei, *Macromol. Rapid Commun.* **2010**, *31*, 10.
[8] a) C. M. Li, L. B. Guo, X. N. He, Z. Q. Hao, X. Y. Li, M. Shen, X. Y. Zeng, Y. F. Lu, *J. Anal. At. Spectrom.* **2014**, *29*, 638; b) H. T. Li, R. H. Liu, S. Y. Lian, Y. Liu, H. Huang, Z. H. Kang, *Nanoscale* **2013**, *5*, 3289; c) Y. Choi, Y. Park, T. Kang, L. P. Lee, *Nat. Nanotechnol.* **2009**, *4*, 742.
[9] T. Petit, L. Zhang, K. E. Peyer, B. E. Kratochvil, B. J. Nelson, *Nano Lett.* **2012**, *12*, 156.
[10] S. M. Azizi, K. Khorasani, *Int. J. Control* **2011**, *84*, 876.
[11] a) Y. Tian, Y. L. Zhang, J. F. Ku, Y. He, B. B. Xu, Q. D. Chen, H. Xia, H. B. Sun, *Lab Chip* **2010**, *10*, 2902; b) T. Kokalj, Y. Park, M. Vencelj, M. Jenko, L. P. Lee, *Lab Chip* **2014**, *14*, 4329.
[12] S. Tottori, L. Zhang, F. M. Qiu, K. K. Krawczyk, A. Franco-Obregon, B. J. Nelson, *Adv. Mater.* **2012**, *24*, 811.
[13] a) C. G. Hu, L. Song, Z. P. Zhang, N. Chen, Z. H. Feng, L. T. Qu, *Energy Environ. Sci.* **2015**, *8*, 31; b) J. Kim, J. K. Koh, B. Kim, J. H. Kim, E. Kim, *Angew. Chem. Int. Ed.* **2012**, *51*, 6864.
[14] B. Kim, H. Shin, T. Park, H. Lim, E. Kim, *Adv. Mater.* **2013**, *25*, 5483.
[15] Q. Ji, M. Miyahara, J. P. Hill, S. Acharya, A. Vinu, S. B. Yoon, J. S. Yu, K. Sakamoto, K. Ariga, *J. Am. Chem. Soc.* **2008**, *130*, 2376.
[16] a) K. Liu, M. Cao, A. Fujishima, L. Jiang, *Chem. Rev.* **2014**, *114*, 10044; b) Y. L. Zhang, Q. D. Chen, Z. Jin, E. Kim, H. B. Sun, *Nanoscale* **2012**, *4*, 4858.

[17] J. S. Randhawa, K. E. Laflin, N. Seelam, D. H. Gracias, *Adv. Funct. Mater.* **2011**, *21*, 2395.
[18] E. Gultepe, J. S. Randhawa, S. Kadam, S. Yamanaka, F. M. Selaru, E. J. Shin, A. N. Kalloo, D. H. Gracias, *Adv. Mater.* **2013**, *25*, 514.
[19] A. A. Solovev, W. Xi, D. H. Gracias, S. M. Harazim, C. Deneke, S. Sanchez, O. G. Schmidt, *ACS Nano* **2012**, *6*, 1751.
[20] N. Bassik, A. Brafman, A. M. Zarafshar, M. Jamal, D. Luvsanjav, F. M. Selaru, D. H. Gracias, *J. Am. Chem. Soc.* **2010**, *132*, 16314.
[21] W. Nakanishi, K. Minami, L. K. Shrestha, Q. M. Ji, J. P. Hill, K. Ariga, *Nano Today* **2014**, *9*, 378.
[22] a) H. B. Jiang, Y. L. Zhang, D. D. Han, H. Xia, J. Feng, Q. D. Chen, Z. R. Hong, H. B. Sun, *Adv. Funct. Mater.* **2014**, *24*, 4595; b) J. Zhang, L. Song, Z. P. Zhang, N. Chen, L. T. Qu, *Small* **2014**, *10*, 2151; c) W. Xiong, Y. S. Zhou, W. J. Hou, L. J. Jiang, Y. Gao, L. S. Fan, L. Jiang, J. F. Silvain, Y. F. Lu, *Sci. Rep.* **2014**, *4*, 6; d) W. Guo, C. Cheng, Y. Z. Wu, Y. A. Jiang, J. Gao, D. Li, L. Jiang, *Adv. Mater.* **2013**, *25*, 6064.
[23] P. Kumar, *RSC Adv.* **2013**, *3*, 11987.
[24] H. H. Cheng, J. Liu, Y. Zhao, C. G. Hu, Z. P. Zhang, N. Chen, L. Jiang, L. T. Qu, *Angew. Chem. Int. Ed.* **2013**, *52*, 10482.
[25] D. D. Han, Y. L. Zhang, H. B. Jiang, H. Xia, J. Feng, Q. D. Chen, H. L. Xu, H. B. Sun, *Adv. Mater.* **2015**, *27*, 332.
[26] Y. L. Zhang, L. Guo, S. Wei, Y. Y. He, H. Xia, Q. D. Chen, H. B. Sun, F. S. Xiao, *Nano Today* **2010**, *5*, 15.
[27] a) K. S. Subrahmanyam, P. Kumar, A. Nag, C. N. R. Rao, *Solid State Commun.* **2010**, *150*, 1774; b) P. Kumar, K. S. Subrahmanyam, C. N. R. Rao, *Int. J. Nanosci.* **2011**, *10*, 559.
[28] a) P. Kumar, B. Das, B. Chitara, K. S. Subrahmanyam, K. Gopalakrishnan, S. B. Krupanidhi, C. N. R. Rao, *Macromol. Chem. Phys.* **2012**, *213*, 1146; b) P. Kumar, L. Panchakarla, C. N. R. Rao, *Nanoscale* **2011**, *3*, 2127; c) K. S. Subrahmanyam, P. Kumar, U. Maitra, A. Govindaraj, K. P. S. S. Hembram, U. V. Waghmare, C. N. R. Rao, *Proc. Natl. Acad. Sci. U.S.A.* **2011**, *108*, 2674; d) K. Gopalakrishnan, K. S. Subrahmanyam, P. Kumar, A. Govindaraj, C. N. R. Rao, *RSC Adv.* **2012**, *2*, 1605.
[29] Y. L. Zhang, L. Guo, H. Xia, Q. D. Chen, J. Feng, H. B. Sun, *Adv. Opt. Mater.* **2014**, *2*, 10.
[30] V. A. Smirnov, A. A. Arbuzov, Y. M. Shul'ga, S. A. Baskakov, V. M. Martynenko, V. E. Muradyan, E. I. Kresova, *High Energy Chem.* **2011**, *45*, 57.
[31] L. Guo, H. B. Jiang, R. Q. Shao, Y. L. Zhang, S. Y. Xie, J. N. Wang, X. B. Li, F. Jiang, Q. D. Chen, T. Zhang, H. B. Sun, *Carbon* **2012**, *50*, 1667.
[32] P. Kumar, K. S. Subrahmanyam, C. N. R. Rao, *Mater. Express* **2011**, *1*, 252.
[33] Y. Matsumoto, M. Koinuma, S. Ida, S. Hayami, T. Taniguchi, K. Hatakeyama, H. Tateishi, Y. Watanabe, S. Amano, *J. Phys. Chem. C* **2011**, *115*, 19280.
[34] C. C. Liu, J. Ju, Y. M. Zheng, L. Jiang, *ACS Nano* **2014**, *8*, 1321.
[35] C. Lee, X. Wei, J. W. Kysar, J. Hone, *Science* **2008**, *321*, 385.
[36] J. W. Suk, R. D. Piner, J. An, R. S. Ruoff, *ACS Nano* **2010**, *4*, 6557.
[37] N. V. Medhekar, A. Ramasubramaniam, R. S. Ruoff, V. B. Shenoy, *ACS Nano* **2010**, *4*, 2300.